International Journal of Biological Macromolecules 191 (2021) 572–583

Contents lists available at ScienceDirect

International Journal of Biological Macromolecules

journal homepage: www.elsevier.com/locate/ijbiomac

Thermoplastic starch nanocomposites using cellulose-rich *Chrysopogon zizanioides* nanofibers

Midhun Dominic C.D. [a,*], Derval dos Santos Rosa [b], Paulo Henrique Camani [b], Athira S. Kumar [a], Neenu K.V. [c], P.M. Sabura Begum [c], Divya Dinakaran [a], Effina John [d], Donna Baby [e], Meenu Mariya Thomas [f], Jaison M. Joy [a], Jyotishkumar Parameswaranpillai [g], Mohammad Reza Saeb [h]

[a] Department of Chemistry, Sacred Heart College (Autonomous), Kochi, Kerala Pin-682013, India
[b] Universidade Federal do ABC, Centro de Engenharia, Modelagem e Ciências Sociais Aplicadas (CECS), CEP 09090-400 Santo André, SP, Brazil
[c] Department of Applied Chemistry, Cochin University of Science and Technology (CUSAT), Kerala Pin-682022, India
[d] Department of Chemistry, St. Albert's College (Autonomous), Kochi, Kerala Pin-682018, India
[e] Department of Chemistry, St. Peter's College, Kolenchery, Kerala Pin-682311, India
[f] Department of Chemistry, Morning Star Home Science College, Angamaly, Kerala Pin-683585, India
[g] School of Biosciences, Mar Athanasios College for Advanced Studies Tiruvalla (MACFAST), Pathanamthitta, Kerala Pin-689101, India
[h] Department of Polymer Technology, Faculty of Chemistry, Gdańsk University of Technology, Gabriela Narutowicza 11/12, 80–233 Gdańsk, Poland

ARTICLE INFO

Keywords:
Cellulose nanofiber
Green composites
Thermoplastic starch
Carbohydrate polymers

ABSTRACT

Green thermoplastic starch (TPS) nanocomposite films aided by cellulose nanofibers (CNFs) from *Chrysopogon zizanioides* roots were developed and characterized. When compared to other lignocellulosic fibers, *Chrysopogon zizanioides* roots revealed exceptionally high cellulose content (~48%). CNFs were separated using an environmentally friendly acid isolation technique that included three stages: (i) alkali treatment; (ii) bleaching; and (iii) mild acid hydrolysis using oxalic acid in an autoclave. Following that, green nanocomposite films were made from potato starch using the solution casting process, by which we used glycerol (30 wt%) to make thermoplastic starch. Then, cellulose nanofibers in different concentrations (0, 1, 2, 3, 4 wt%) were added to the thermoplastic starch matrix. The isolated CNFs had diameters in the range of 17–27 nm. Besides, these nanostructures presented a very high crystallinity index (~65%), thereby enhanced the thermal stability. TPS/CNF green nanocomposites containing 3 wt% CNFs had exceptional tensile strength (~161%), tensile modulus (~167%), thermal stability, and crystallinity. As a result, nanocomposite films made of starch and cellulose nanofibers (3 wt%) extracted from *Chrysopogon zizanioides* roots would be alternatives for sustainable packaging. It can be concluded that *Chrysopogon zizanioides* roots have high potential for polymer industry.

1. Introduction

The study of biocomposites and their relationship with environmental sustainability are in high demand nowadays. Traditional plastics have posed a hazard to the environment by contaminating land and water. Green technologies have become important as a result of increased manufacturing and usage of plastics, without endangering the environment [1]. Big companies have competed in green plastics and green composites due to the production of eco-friendly materials in the last decade, covering commercial and engineering applications and techno-economic benefits [2,3]. Nanocellulose derived from plant fibers has been extensively researched and recommended as a semi-structural fiber replacement in the composite industry. Because of their biodegradability, environmental friendliness, and sustainability, entirely green biocomposites made from nanocellulose have also taken a big hit. In 2015, of the plastic wastes generated, only 9% was recycled, 12% was incinerated, and 79% was disposed of in landfills [3]. As a result, green composites based on nanocellulose offer a viable alternative to traditional plastic packaging.

Cellulose is the most abundant polysaccharide in the world, present on the plant cell wall, and it consists of β-D-glucopyranose units linked by (1–4) glycosidic bonds [4]. It exists in microfibrils that contain tightly

* Corresponding author at: Department of Chemistry, Pandit Karuppan Road, Sacred Heart College (Autonomous), Thevara, Kochi, Kerala Pin-682013, India.
E-mail address: midhundominic@shcollege.ac.in (M. Dominic C.D.).

https://doi.org/10.1016/j.ijbiomac.2021.09.103
Received 3 July 2021; Received in revised form 14 September 2021; Accepted 15 September 2021
Available online 25 September 2021

bound non-cellulosic components like hemicellulose, lignin, and pectin [5,6]. The isolation of nanocellulose from different sources was the subject of many reports [7]. Before nanocellulose isolation, alkali treatment and bleaching are done as pre-treatment to eliminate the non-cellulosic components such as hemicellulose and lignin and other cementing particles typically present within the samples [8]. Then, various physical and chemical methods have been employed for the extraction/isolation of nanocellulose, among which the important reports are discussed as follows. Mahardika and co-workers [9] isolated nanocellulose from pineapple leaves by chemical pre-treatment, followed by high-shear homogenization and ultrasonication. The extracted nanocellulose showed better crystallinity and thermal stability compared to the raw fiber. De Campos and co-workers [10] adopted an enzymatic treatment of the bleached fibers (sugarcane bagasse and curaua fibers), followed by sonication to prepare nanofibers. Even though the method is eco-friendly, the crystallinity index of the bleached fiber was reduced after enzymatic and sonication processes. Ali and co-workers; Ravindran, Sreekala, and Thomas; and Rajinipriya and co-workers studied the effect of ball milling on the preparation of nanocellulose from treated maize cobs [11], treated pineapple leaves [12], and treated carrot pulp [5], respectively. Overall, ball milling appeared as a viable and eco-friendly method for the extraction of nanocellulose.

Besides, grinding, cryo-crushing [13], and mechanical shearing [14] were also used to isolate nanocellulose. The general consequence of mechanical methods is that they damage the fibrous nature of cellulose. Acid hydrolysis is an easy, efficient, and economical method to remove non-cellulosic components from the fiber. Generally, one of the most commonly used acids is sulfuric acid, besides hydrochloric acid, nitric acid, or some acid mixtures that have been used to extract nanocellulose [15]. Several works have been reported on mineral acid hydrolysis of natural fiber [16]. High crystallinity is an exceptional feature of the nanocellulose produced from mineral acid hydrolysis. The acid hydrolysis could remove the amorphous region and leave the crystalline region unaltered [17]. In addition, the mineral acid transition metal-catalyzed hydrolysis to produce nanocellulose is also reported [18]. However, the use of strong acids has several disadvantages, e.g., corrosion to the instruments, and also the disposal of waste acid is problematic. Consequently, the replacement of this corrosive and eco-polluting mineral acid by a greener one is highly acknowledged. Since oxalic acid is mild, hydrolysis using this acid in an autoclave was proposed. Interestingly, the steam explosion and acid hydrolysis impart nano dimensions to the fibers [19]. Thus nanocellulose can be successfully isolated by the steam explosion method [20].

Starch is a commonly used biopolymer to develop thermoplastic starch due to its easy availability, low cost, high potential application range, and other characteristics. Starch in its native form is converted into thermoplastic by the addition of plasticizers (glycerol, citric acid, and sorbitol) [21]. Starch, as such, has poor water resistance and mechanical properties [22]. As a solution, the plasticizer incorporation reduces the crystallinity but improves the overall performance of the starch [23]. Thermoplastic starch (TPS) is a material produced from a structural disturbance that occurs in the interior of starch granules in the presence of plasticizers [24]. Dufresne's group investigated the effects of cellulose microfibril content, relative humidity, and glycerol (plasticizer) on the mechanical and water sorption properties of TPS [25]. Recently, researchers have demonstrated that nanocellulose can be used to increase the mechanical performance of TPS [26,27]. Balakrishnan et al. [28] reported that UV resistant transparent bionanocomposite films with excellent mechanical and barrier properties can be achieved by the addition of 3 wt% CNFs into the starch matrix. Cerqueira and co-workers discussed the feasibility of incorporating cellulose nanocrystals from coconut fibers in starch nanocomposites [29]. They used glycerol as a plasticizer and reported enhanced barrier and mechanical properties upon incorporating nanocellulose in the polymer matrix. Coelho and co-workers prepared cellulose nanocrystals from grape pomace, incorporated them in starch, improved the tensile strength, Young's modulus, and water vapor barrier of the starch film [30]. Nordin and co-workers obtained micro cellulose fibers from dried cellulose pulps and incorporated them in TPS [31]. They observed an excellent improvement in biocomposites' thermal and mechanical properties due to the excellent adhesion and strong intermolecular interaction between the micro cellulose fibers and TPS. Santana and co-workers introduced CNFs extracted from sisal fiber into cassava starch plasticized with glycerol [32]. Their composite showed lower swelling and water vapor permeability but higher tensile strength and Young's modulus compared to reference starch; therefore, they concluded that the developed biocomposite could be intended for packing applications.

Various sub-classes of carbohydrate polymers have been found in plants, grasses, trees and vegetables and used in diverse fields, yet there are still several green resources that have never been explored. In this regard, continued attempts have been made to find complements to carbohydrates obtained from the root of grasses or vegetables. What sustainability and circular economy concepts suggest is to find the best complement by a thorough examination of pairs of natural sources. Even though there are several documents reported in the literature [33] that deal with the extraction, structural characterization, and applications of plant fibers such as bast fibers, seed fibers, and leaf fibers, no detailed investigations have been done so far on root fibers. *Chrysopogon zizanioides*, commonly known as vetiver is an Ayurvedic medicinal plant often found in Kerala, India. It is a perennial bunchgrass of the poaceae family. It has strong fibrous roots that can grow up to 4 m deep. Donjadee and co-workers investigated the effect of vetiver grass clippings as mulch in reducing soil erosion and water runoff [34]. Vetiver grass can absorb harmful elements and heavy metals and is a key biological filter of industrial wastewater [35]. The roots of vetiver are usually used for the extraction of essential oil (vetiver oil), used to manufacture perfumes, agarbathis, soaps, cosmetics etc. By 2022, the global vetiver oil market might be worth US$ 169.5 million [36]. In India, about 20–25 t of vetiver oil are produced each year [37]. The roots left over after vetiver oil extraction might be considered agro-waste that can be transformed into a value-added product such as nanocellulose. The cellulose content of raw *Chrysopogon zizanioides* roots (48%) is significantly higher than that of Cassava roots (6.7%) and carrots (10.01%) [38,39]. Isolating CNFs from *Chrysopogon zizanioides* roots for the development and characterization of TPS/CNF biocomposites appears to be a good approach from a chemistry and engineering standpoint. No previous work on the extraction of CNFs from *Chrysopogon zizanioides* roots and their reinforcement in TPS biocomposites has been reported to the author's knowledge. For the isolation of CNFs, only mild agents is utilized. To reduce potential environmental repercussions, chlorite bleaching is replaced by hydrogen peroxide, and harmful sulfuric acid in acid hydrolysis is substituted by oxalic acid, making the process more eco-friendly. Potato starch and glycerol were used to make a TPS composite, which was subsequently reinforced with CNFs. The TPS/CNFs biocomposite was made using the solution casting approach [28]. As a result, we propose a novel use for the roots of *Chrysopogon zizanioides*, a cellulose-rich resource that can be used to replace synthetic plastic/fiber-based packing materials with totally green nanocellulose-based starch thermoplastics. Only a small amount of CNFs (1–4 wt%) was employed to manufacture starch-based sustainable biocomposite films with good mechanical and thermal properties.

2. Materials and methods

2.1. Materials

The raw *Chrysopogon zizanioides* roots were collected from the Ayurvedic medical shops of Kodungalloor, Kerala, India. All the reagents and chemicals such as NaOH (A.R. 98%), H_2O_2 (30% *W/V*), $C_2H_2O_4$ (A.R. 99.8%), KOH (A.R. 85%), potato starch (23% amylose content), and glycerol (98%) were purchased from Nice Chemicals Private Limited, Kerala, India.

Table 1
Acronyms and definitions of samples for each stage of this work.

Acronyms	Definition of samples
RCZ	Raw sample
ACZ	Alkali-treated sample
BCZ	Bleached sample
CNF	Cellulose Nanofiber
Neat starch	Thermoplastic starch (TPS)
TPS/CNF 1	Composite film of thermoplastic starch containing 1 wt% of CNFs
TPS/CNF 2	Composite film of thermoplastic starch containing 2 wt% of CNFs
TPS/CNF 3	Composite film of thermoplastic starch containing 3 wt% of CNFs
TPS/CNF 4	Composite film of thermoplastic starch containing 4 wt% of CNFs

2.2. Methods

The methodology for the preparation of composites involves two stages: isolation of cellulose nanofibers and preparation of TPS/CNF nanocomposite films. Table 1 presents some acronyms and definitions for each sample of two stages.

2.2.1. Isolation of cellulose nanofibers

Chrysopogon zizanioides roots were collected, cleaned, dried, and cut into small pieces of 1 cm. About 100 g of the raw sample (RCZ) was treated with 2% NaOH solution (1:10 g/mL) in an autoclave to remove hemicellulose and lignin. The process was repeated two times. The sample was washed well, and the alkali-treated sample (ACZ) was bleached with 1000 mL 15% H_2O_2 (*w/v*) and 100 mL 10% NaOH solution. The bleaching process was repeated four times for whitening the sample. The bleached sample (BCZ) was washed thoroughly with distilled water and then treated with 1000 mL, 5% oxalic acid (w/v) in an autoclave at 15 psi and kept under this pressure for 15 min, and the pressure was suddenly released. The process was repeated two times. The resultant sample was washed well to remove excess acid, and it was homogenized (D lab make homogenizer model D-500) in distilled water for one hour to get a refined suspension of CNFs.

2.2.2. Preparation of TPS/CNF nanocomposite films

The solution casting method was used for the development of biocomposites. Pre-weighed potato starch was dissolved in 100 mL of hot distilled water, and 30% of glycerol (on dry starch basis) was added drop-wise and stirred thoroughly by a mechanical stirrer. The 30% of glycerol was chosen because it was being widely used in the literature, improving elasticity and promoting the movement of the starch chains, thus increasing the flexibility [21]. The CNF suspension was sonicated for 15 min before use. The required amount of CNF suspension (total solid content of 0.9%) was added to the above solution and stirred well using a mechanical stirrer at 700 rpm for 30 min at a temperature of 90 °C. Then, the obtained viscous solution was cast onto a glass plate and kept in an air oven for 12 h at about 50 °C [21]. Likewise, films with 0, 1, 2, 3, 4 wt% of CNFs (based on the dry weight of starch) were prepared using a solution casting technique. The dried films were stored in a plastic bag at 25 °C and 60% relative humidity for a week before characterization [23].

2.2.3. Characterizations

The chemical composition at each stage of isolation of CNF was analyzed using ASTM standards, cellulose (ASTM D 1103-55T), hemicellulose (ASTM D 1104-56), and lignin (ASTM D 1106-56). The Fourier Transform Infrared Spectroscopy-Attenuated Total Reflectance (FTIR-ATR) spectra of the samples were determined using Thermo Nicolet Avatar 370 model FTIR spectrophotometer (Waltham, MA, USA). The data acquisition was carried out in a range of 400–4000 cm^{-1}, 32 scans, and with 4 cm^{-1} spectral resolution. X-ray diffraction analysis (XRD) was conducted by Bruker D8 Advance X-ray powder diffractometer (Bruker, MA, USA). The crystallinity index (*IC*) of RCZ, ACZ, BCZ, and CNFs were calculated using Segal Eq. (1):

Table 2
The chemical composition of fibers after each stage of chemical treatment.

Sample	Cellulose (%)	Hemicellulose (%)	Lignin (%)
RCZ	48 ± 3	28 ± 3	23 ± 2
ACZ	61 ± 4	15 ± 2	11 ± 2
BCZ	87 ± 3	4 ± 0.5	3 ± 0.5

$$I_C(\%) = \left(1 - \frac{I_{am}}{I_{200}}\right) \times 100\% \quad (1)$$

where I_{200} is the intensity of diffraction of the (200) lattice peak (~2θ = 22.8°), and I_{am} is the intensity from the amorphous phase (~2θ = 18.6°). The morphological studies of the samples were obtained using Joel 6390 LA scanning electron microscopy (SEM) and high-resolution transmission electron microscopy (TEM), Joel/JEM 2100, (JOEL USA, Inc., Peabody, MA, USA). The particle size confirmation was done using the Malvern Zetasizer Nano series with a 4 mW 632.8 nm laser. Three replications were done for the analysis. Thermogravimetry analysis (TGA) was performed on Perkin Elmer STA 600 (Waltham, USA), at a temperature range of room temperature to 750 °C in the N_2 atmosphere at a heating rate of 10 °C/min, in N_2 flow 20 $mlmin^{-1}$. In addition, differential scanning calorimeter (DSC), Netzsch DSC 204 F1 (Germany), was used to carry out DSC analysis in an inert nitrogen atmosphere at a temperature range of room temperature to 400 °C at a heating rate of 10 °C/min. The stress-strain analysis was conducted on Shimadzu Model AGI Universal Testing Machine according to ASTM D 412.

3. Results and discussions

3.1. Characterization of raw and treated fibers and cellulose nanofibers (CNFs)

3.1.1. Chemical composition of raw and treated fibers

The composition of the samples at each stage of the chemical treatments was determined and summarized in Table 2.

Initially, 48% of cellulose was found in the raw sample (RCZ), and an increase in the cellulose content on successive chemical treatments could be detected. Alkali treated sample (ACZ) has about 61% cellulose, and that of the bleached sample (BCZ) has 87% cellulose. A remarkable reduction in the hemicellulose and lignin content from 28% to 4% and from 23% to 3% implies the effectiveness of the adopted methodology. Chemical modification and pre-treatments on the fiber surfaces enhance its properties. The NaOH treatment and H_2O_2 bleaching are adopted as pre-treatments for the fibers to remove the samples' non-cellulosic components and improve the fiber-matrix interface. Alkali treatment effectively removes the hemicellulose, lignin, pectin, wax, and other components, acting as cementing materials within the plant cell wall. The successive removal of these materials imparted surface roughness and enhanced mechanical bonding [40,41]. Herein, NaOH with low concentration was used for the mercerization process. The overuse of alkali results in fiber damage and lower stability [40] and cellulose degradation [20]. The bleaching process was performed to ensure the complete removal of non-cellulosic components like lignin and an increase in the cellulose content. Cherian and co-workers suggested removing lignin on bleaching depends on the type of lignin present, either as alkali sensitive or alkali resistant. Lignin degrades to different polar groups such as carboxylic acid, hydroxyl groups, and others on bleaching in the presence of alkaline medium. This ensures more availability and exposure of cellulose. Bleaching also imparts whiteness to the sample [42] and helps in diminishing the particle size. Peroxide bleaching adopted in the methodology may also reduce the risk of environmental impact by using chlorite bleaching. Chirayil et al., reported a similar observation which implies the alkali treatment,

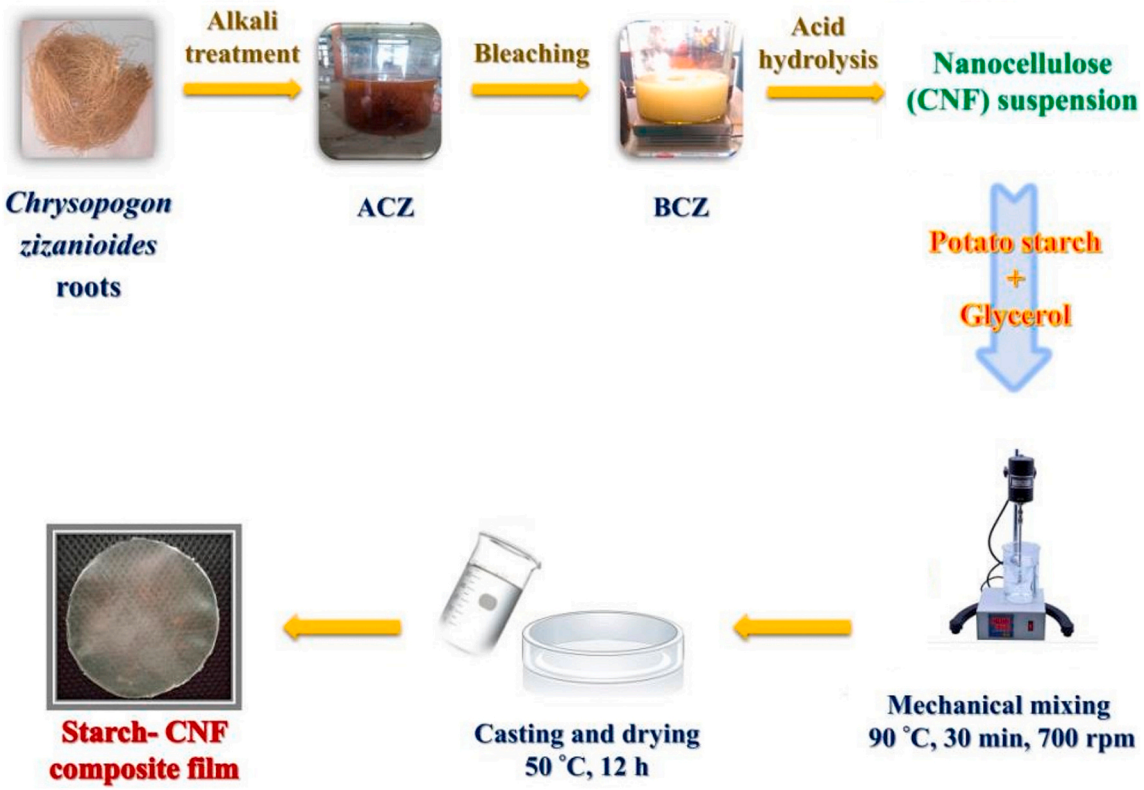

Fig. 1. Different stages in the preparation of TPS/CNF bionanocomposite film.

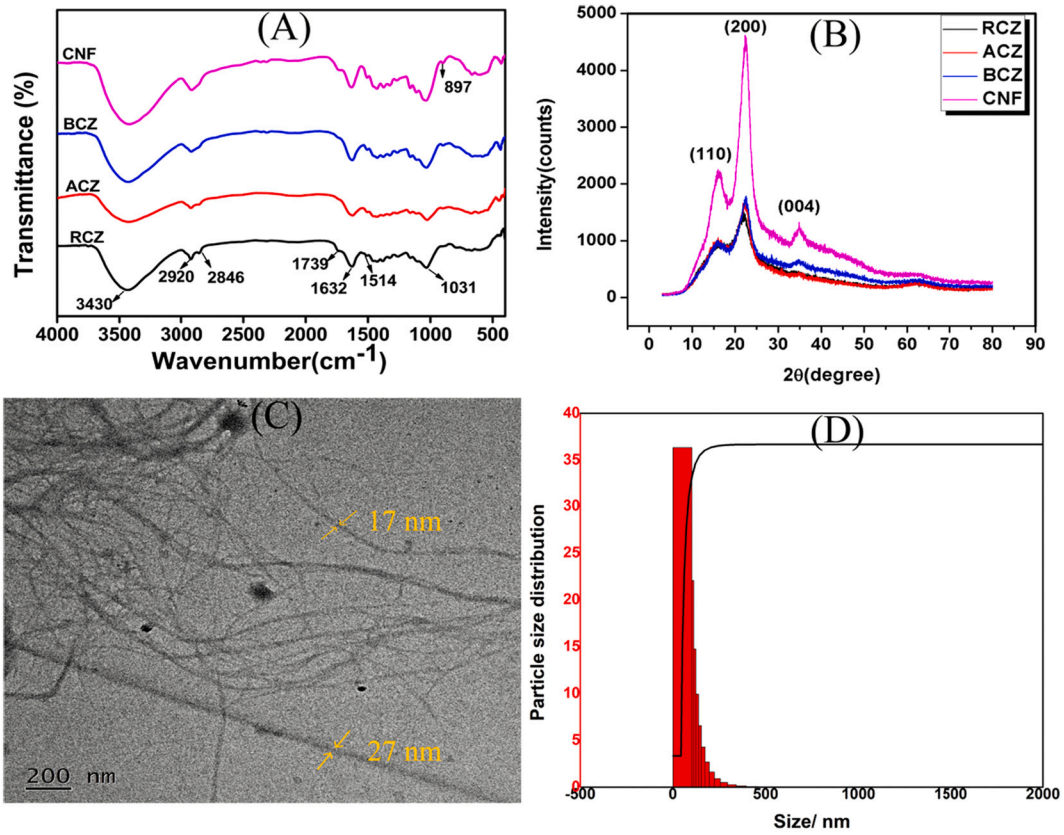

Fig. 2. (A) FTIR spectra of samples (RCZ to CNF), (B) XRD pattern of samples (RCZ to CNF), (C) TEM image of CNFs, and (D) DLS spectra of CNFs.

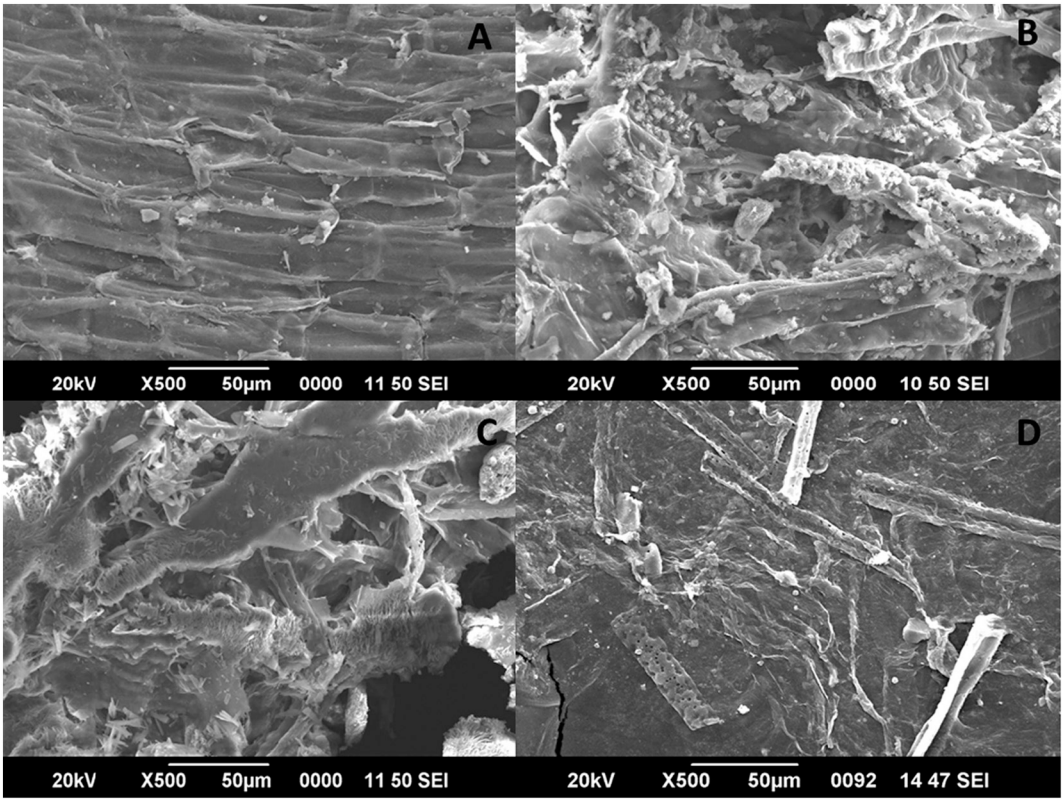

Fig. 3. SEM images of (A) RCZ, (B) ACZ, (C) BCZ, and (D) CNFs.

followed by bleaching, resulting in hemicellulose hydrolysis to sugars and lignin depolymerization to phenolic compounds, which are soluble in water [19]. Cherian and co-workers investigated the depolymerization mechanism using the steam explosion method. The steam explosion results in the partial breakage of the hydrogen bonds within the glucopyranose unit at C3 and C6 position [20]. The sudden pressure release in the steam explosion method may also lead to rapid depolymerization and defibrillation. The low concentration of NaOH solution (2%), hydrogen peroxide bleaching (avoiding chlorite bleaching), and oxalic acid hydrolysis of bleached fiber in the autoclave (avoiding sulfuric acid hydrolysis) make the proposed nanocellulose extraction process greener and eco-friendly. Fig. 1. shows the different stages of the preparation of TPS/CNF bionanocomposite film.

3.1.2. *Chemical structure of raw and treated fibers*

The FTIR spectra of RCZ, ACZ, BCZ, and CNFs are shown in Fig. 2A. The chemical structure and changes in the functional groups' position were obtained from the FTIR spectra. The fibers contain both cellulosic and non-cellulosic components. These constituents contain hydroxyl groups, ester, and ether linkages. The disappearance and increasing intensity of specific bands in the FTIR spectra shows the removal and modification of fiber components after successive chemical treatment [43]. A band at 3430 cm^{-1} is observed in the spectra of Fig. 2A, being the characteristic of O—H stretching vibrations [44]. This absorption band indicates inter and intra-molecular hydrogen bonds in the cellulose fibers [45]. Besides, other peaks in the range of 2920 cm^{-1} are observed, corresponding to aliphatic C—H stretching in cellulose [46]. However, RCZ exhibits a band at 2846 cm^{-1}, attributed to the stretching vibrations of -OCH_3 groups present in lignin and hemicellulose [47]. The disappearance of the peak at 2846 cm^{-1} in the prepared CNFs implies the efficiency of alkali treatment, bleaching, and acid hydrolysis in eliminating lignin and hemicellulose.

In addition, a band at 1739 cm^{-1} could be observed in the case of RCZ due to the C═O stretching vibrations of hemicelluloses and lignin [46]. This band was found to be decreasing in intensity after successive chemical treatment, showing the removal of lignin and hemicellulose. The absence of the peak at 1514 cm^{-1} (C═C vibrations) in CNFs indicates the complete removal of lignin-containing aromatic rings [48]. The peak at 1632 cm^{-1} could indicate O—H bending of water absorbed in the case of RCZ, ACZ, BCZ, and CNFs, or it could indicate the hydrophilic nature of the fibers [49]. Other bands were also observed in the spectra, shown in Fig. 2A. The band at 1031 cm^{-1} is attributed to C—O stretching vibrations in cellulose. The band at 897 cm^{-1} is characteristic of the cellulosic structure due to the 1, 4-β glycosidic linkage. This band got intensified on successive chemical treatment and became more prominent in the case of CNFs, indicating the isolation of cellulosic fibers [43]. Thus, the chemical treatment improved the cellulose content in the fibers by removing non-cellulosic components, exposing more cellulose crystalline phase, and producing cellulose nanostructures without loss of the prominent chemical structure of cellulose.

3.1.3. *Crystallinity of raw and treated fibers*

The crystallinity and crystalline structure of RCZ, ACZ, BCZ, and CNFs were studied using X-ray diffraction analysis. The XRD spectra of RCZ, ACZ, BCZ, and CNFs were shown in Fig. 2B. The XRD pattern of CNFs showed peaks at 2θ values equal to 15.7°, 21.7°, and 34°, that corresponds to the reflection planes (110), (200), and (004) respectively, owing to cellulose Type I structure. These values agree with Dai and co-workers' studies [46] and Trilokesh and co-workers [50]. Foner and Adan reported a principal peak at $2\theta = 22.5°$ and secondary peaks in the range of 14.5° and 16.3° for cellulose Type I structure [51]. The sharp, intense peaks were obtained for CNFs at the corresponding 2θ values, implying the higher crystallinity of the extracted CNFs [43]. The sharp peak at 2θ value equal to 21.7° implies crystalline cellulose in CNFs [45]. It is worth pointing out that similar XRD patterns were obtained for all the samples studied, and it indicates the efficacy of the chemical treatments in maintaining the chemical structure of natural fibers throughout the isolation process. Abraham and co-workers

Table 3
Comparison of the fiber diameter, crystallinity index, and yield of the prepared CNFs with reported works in the literature.

Source	Method of synthesis	Yield (%)	Crystallinity Index (%)	Diameter (nm)	Reference
Helicteres isora	Acid hydrolysis (10% $C_2H_2O_4$) and steam explosion	48	90	20	[19]
Cassava root peelings and bagasse	Acid hydrolysis (30–50% H_2SO_4)	12.3, 10.5	71.1–92.6	2.3–5.4	[38]
Rose stems	Acid hydrolysis (0.1 L of 300 g/L H_2SO_4)	17.2	22.2	30	[62]
Apple stems	Acid hydrolysis (9.17 M H_2SO_4)	5.2	69.1	10–20	[63]
Millet waste	Acid hydrolysis (2 M HNO_3)	50	55	–	[64]
Banana peels	Acid hydrolysis (1% H_2SO_4) and high pressure homogenization	5.1	64.9	10.9–22.6	[65]
Cocos nucifera	Acid hydrolysis (80% CH_3COOH and 70% HNO_3) and ball milling	74.2	77.8	55–64	[66]
Ramie	Ultrasonication	89.35	73.65	9.9–89.1	[67]
Bamboo	Ultrasonication	65–70	69.02	10–40	[68]
Wheat	High pressure homogenization	55.6	57.20	14.01	[69]
Chrysopogon zizanioides roots	Steam explosion followed by acid hydrolysis and homogenization	45–50	65.08	17–27	Current work

observed a left shift of the principal peak on steam-exploded alkali-treated fibers due to the transformation from cellulose I to cellulose II and their co-existence [52]. In the current study, there is no shift of the principal peak in the XRD pattern also contributes to the conformation of cellulose I in the fibers tested.

Cellulose comprises amorphous and crystalline regions, and the removal of the amorphous region increases the crystallinity of the sample [53]. The crystallinity index of RCZ, ACZ, BCZ, and CNFs were calculated using the Segal equation (Eq. (1)), and the values obtained are 43.06%, 51.58%, 56.18%, and 65.08%, respectively. At every stage of extraction, an increment in the crystallinity index could be observed. The lower value of the crystalline index was obtained for raw fiber, which implies more amorphous regions in the sample due to the presence of hemicellulose, lignin, and waxes. Besides, the crystalline peak at the (200) plane in all the samples was preserved, and its intensity increased for CNF. Thus, this effect implies that the chemical treatments (alkali treatment, bleaching, and acid hydrolysis) remove only the amorphous phase, while the crystalline phase remains unaltered [45]. Apart from the increased crystallinity, removing the amorphous phase during the progressive chemical treatments also reduces the size of the cellulose from macro to nanoscale. Besides, crystallinity increases the rigidity, thermal stability, and strength of the CNFs [49].

3.1.4. Morphology of RCZ, ACZ, BCZ, and CNFs

In the development of composites, morphological structure and fiber properties are important for predicting the interactions of the fiber with the polymer matrix. Scanning electron microscopy (SEM) was performed to study the morphological characteristics of different stages of *Chrysopogon zizanioides* fibers. The changes in the morphology of fibers in each stage of chemical treatment are shown in Fig. 3. The surface of RCZ (Fig. 3A) is found to be uneven and it consists of bundles of individual cells that are tangled with cementing materials like lignin and hemicellulose. A noticeable change in the surface morpholology of RCZ is observed when the raw fiber is treated with NaOH solution. The surface morpholology of ACZ is shown in Fig. 3B. The surface of ACZ shows numerous tiny pores and openings. These voids are created by the dissolution and leaching out of cementing materials like hemicellulose, lignin, and waxes during the mercerization process. The alkali treatment also makes the fibers more rigid and stiff. Dominic et al. reported a similar observation when rice husk is treated with NaOH solution [54]. The mercerization process not only increases the stiffness of the fibers but also increases the number of reactive sites on the fiber surface which favours fiber wetting [55]. The voids produced on the surface of ACZ provide greater mechanical anchoring and interlocking of the fiber with the polymer matrix. The surface morphology of the bleached fiber (BCZ) is shown in Fig. 3C. The surface of BCZ is found to be smoother compared to the surfaces of RCZ and ACZ. Ireana et al. reported a similar observation when oil palm empty fruit bunches are bleached with alkaline hydrogen peroxide solution [56]. Defibrillation and size reduction of fibers happen up on bleaching. The surface morphology of the isolated CNFs is shown in Fig. 3D. The image shows that individual defibrillation has taken place after acid hydrolysis and homogenization. Panyasiri and co-workers [57] reported a similar fibrous structure in CNFs extracted from cassava bagasse due to the removal of plant residues and impurities. The SEM micrographs demonstrate the efficiency of acid hydrolysis combined with the steam explosion, which results in the formation of individual fibers and can be employed as a reinforcing filler in various matrices.

The evidence on the isolation of nanocellulose from *Chrysopogon zizanioides* roots was confirmed by transmission electron microscopy (TEM) image as shown in Fig. 2C. The obtained fiber diameter was approximately between 17 and 27 nm. TEM image demonstrated the well-arranged thread-like network image of CNFs with aggregations. Panyasiri and co-workers [57] suggest that the aggregations of fibers are the sign of strong hydrogen bonds between the fibers. The presence of hydrogen bonds also implies the hydrophilic nature of the CNFs [8].

Furthermore, the fine filament-shaped CNFs show the removal of tightly wrapped hemicellulose, lignin, and wax in the fibers by the alkali treatment, bleaching, and acid hydrolysis [14]. That means the chemical treatments caused the isolation of cellulose fibers due to the removal of amorphous material. In other words, the chemical treatments facilitated depolymerization of the cellulose molecules and provided fibrillar nature to each fiber, which possesses strong hydrogen bonding [58]. These findings indicate the successful isolation of cellulose nanofibers from *Chrysopogon zizanioides* roots and the effectiveness of the steam explosion method. It is essential to establish morphology –property correlation while studying the reinforcing effect of CNFs in the polymer matrix. Kumagai et al. reported that low fibrillated CNFs (diameter > 10 μm) showed very weak reinforcement while the high-fibrillated CNFs (diameter < 0.1 μm) considerably enhanced modulus and tensile strength of polymer composites [59]. It is difficult to determine the actual length of the prepared CNFs from the TEM analysis. From Fig. 2C, the length of the isolated CNFs is in the micro meter range and the diameter is in the range of 17–27 nm. Thus, the prepared CNFs have a high aspect ratio. Hu et al. reported that for fibers with similar diameter better reinforcement is shown by the one which is having a higher aspect ratio [60]. So, the TEM analysis proves the reinforcing potential of the isolated CNFs in the polymer matrix.

Dynamic light scattering (DLS) spectra provided information on the fiber diameter. The DLS spectra of CNFs are shown in Fig. 2D. The DLS analysis confirmed the nano-dimension and fiber diameter of the isolated CNFs obtained from SEM and TEM analysis. The structural information about the CNFs could not be obtained from the DLS spectra. However, the hydrodynamic particle size is determined from the DLS analysis [44]. From the DLS spectra, the diameter of CNFs is in the nanoscale, confirming the complete conversion of cellulose segments to nanocellulose [61]. The DLS spectra of the isolated CNFs show narrow size distribution and the average diameter of CNFs is found to be around 40 nm. Dominic et al. reported a similar DLS spectra for CNFs isolated from rice husk [54]. The yield of the isolated CNFs is calculated to be 45%. The yield of the isolated CNFs is found to be comparable with that of CNFs obtained from *Helicteres isora* plant [19]. Table 3 compares the

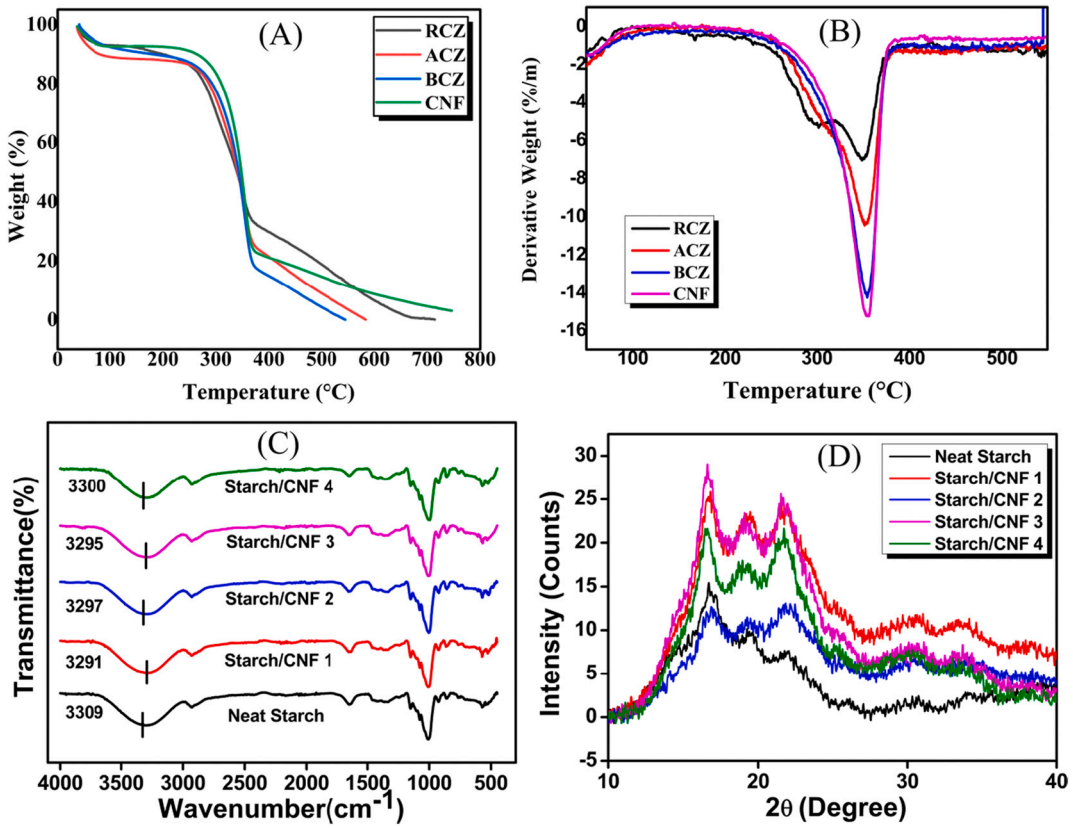

Fig. 4. (A) TG curves of samples (RCZ-CNFs), (B) DTG curves of samples (RCZ-CNFs), (C) FTIR-ATR spectra of TPS/CNF composites, and (D) XRD pattern of TPS/CNF composites.

Table 4
Thermal properties of RCZ, ACZ, BCZ, and CNFs.

Sample	T_{10} (°C)	T_{50} (°C)	T_{max}(°C)	Residue at 500 °C (%)
RCZ	176	338	348	18.71
ACZ	168	340	351	8.87
BCZ	139	342	354	4.22
CNF	250	347	355	14.56

fiber diameter, crystallinity index, and yield of the isolated CNFs with reported works in the literature.

3.1.5. *Thermal stability of RCZ, ACZ, BCZ, and CNFs*

The thermal stability of RCZ, ACZ, BCZ, and CNFs were studied using the thermogravimetric method. The thermogravimetric analysis (TGA) monitors the change in mass of the fibers as a function of temperature. The TG and DTG curves of RCZ, ACZ, BCZ, and CNFs are shown in Fig. 4. From Fig. 4A, it is possible to conclude that the initial weight loss occurred at ~100 °C in all the samples is due to the evaporation of bonded water molecules and other volatile materials present in them [53]. This weight loss implies the hydrophilic nature of the cellulose fibers [44]. From the TG curve, the significant weight loss of the tested fibers occurred between 250 °C to 450 °C. On the other hand, from the DTG curve (Fig. 4B) the primary decomposition peak at higher temperature and a secondary decomposition peak at a lower temperature for RCZ and ACZ samples was observed. The secondary decomposition peak at a lower temperature (190 °C) is due to weight loss corresponding to the decomposition of non-cellulosic components such as hemicellulose and pectin [48]. The secondary decomposition peak was absent in CNFs, suggesting that the non-cellulosic components are entirely removed from nanocellulose. The primary decomposition (T_{max}) was at ~350 °C, being due to the decomposition of cellulose [70].

Table 4 shows the temperature at 10% degradation (T_{10}), the temperature at 50% degradation (T_{50}), the temperature at which maximum degradation (T_{max}), and the residue at 500 °C of RCZ, ACZ, BCZ, and CNFs, respectively. From Table 4, it is clear that the T_{10}, T_{50}, and T_{max} of the CNFs were increased compared to RCZ, ACZ, and BCZ. T_{10}, T_{50}, and T_{max} of CNFs are high values due to removal of non-cellulosic components from CNFs during the chemical treatment [48]. The residual content is the highest for the RCZ. It is due to high plant residues and ash content [67]. The residual ash content gradually decreased on alkali-treated and bleached fibers. However, CNFs showed considerably larger ash than ACZ and BCZ due to the increased crystallinity of CNFs [48]. Thus, it is clear that the thermal stability of CNFs was increased compared to the others samples. The higher value of T_{max} for CNFs points to the usefulness of the steam explosion method for extracting CNFs. The thermal stability of CNFs is mainly due to the crystalline domains present in them. Therefore, the high thermal stability of CNFs leads to a wide range of applications, including biocomposites.

3.2. *Characterization of TPS/CNF nanocomposites*

3.2.1. *Fourier transform infrared spectroscopy (FTIR-ATR)*

The better interaction between the matrix phase and the reinforcing filler was confirmed using FTIR-ATR spectroscopy. Fig. 4C shows the FTIR spectra of neat TPS and TPS/CNF composites. An almost similar patterned spectrum was obtained as the matrix, and the filler is identical polysaccharides with the same functionalities. The broadband range of 3500–3200 cm^{-1} in the neat TPS film and composites were observed, corresponding to the –OH stretching vibrations. It indicates inter and intra-molecular hydrogen bonding [71]. Compared to neat TPS film, there is a shift of peak value of –OH stretching vibrations to lower wavenumber in the case of TPS-cellulose nanocomposites. Zhang and co-workers reported that the decrease in frequency indicates new hydrogen

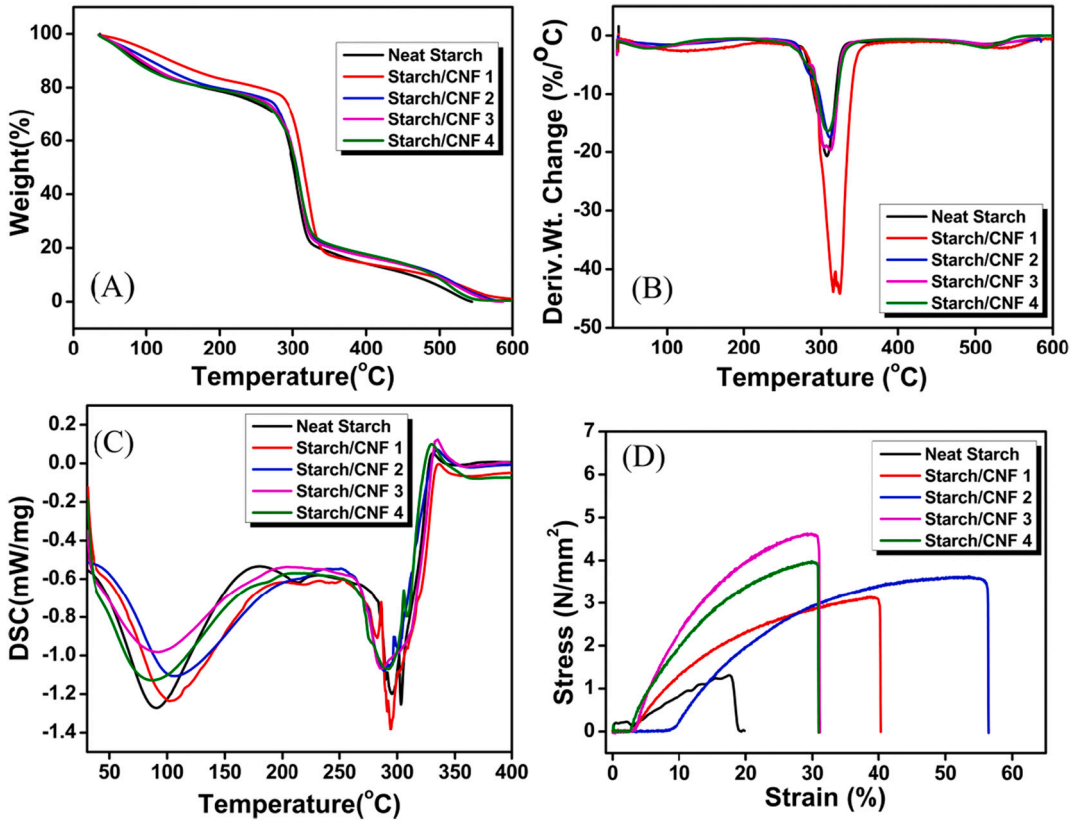

Fig. 5. (A) TG curves of TPS/CNF composites, (B) DTG curves of TPS/CNF composites, (C) DSC curves of TPS/CNF composites, and (D) Stress-strain curves of TPS/CNF composites.

bonds between the starch and the filler [72]. On the other hand, an increase in the bonding ensures better compatibility of the films. Besides, it also represents the better reinforcing effect of cellulose in the matrix. A peak at 2941 cm^{-1} in all composite films was observed, being ascribed to aliphatic C—H stretching [73], and the presence of the peak at 1650–1640 cm^{-1} corresponds to that of absorbed water [71]. Owi and co-workers asserted this peak as the characteristic peak of the starch molecules, which explains its hydrophilic nature [74].

Other peaks are also observed in TPS and biocomposites films. A peak at 1154 cm^{-1} corresponds to the CO stretching vibrations due to the presence of glycosidic bond in the starch film and the TPS-cellulose nanocomposites [75]. This peak, along with the peak at 1010–990 cm^{-1}, is associated with the anhydroglucose ring present in the starch molecule and can also be related to glycerol molecules [71]. A slight shift of this specific peak to a lower wavenumber for nanocomposites than the neat starch film was visible in the spectra. Karimi and co-workers reported that the peak shift corresponds to new interactions between the TPS and cellulose molecules [76]. All the peaks below 1000 cm^{-1} in the prepared composites arose due to glucose molecule, which is the primary constituent of starch and cellulose [28]. Due to the similar molecular structure of starch and cellulose, comparable spectra were obtained in the prepared samples. However, the shift of specific bands implied a better interaction between the polymer and reinforcing filler via hydrogen bonding.

3.2.2. Crystallinity of TPS/CNF Nanocomposites

X-ray diffraction analysis was carried out to study the incorporation of CNFs in the TPS matrix. The X-ray diffraction pattern of TPS/CNF composites is shown in Fig. 4D. The prominent peaks at 17°, 19°, 22°, and 31° are the characteristic peaks of TPS. The peaks correspond to 17°, 19°, and 22°, corresponding to EH-type and VH-type structures. The EH-type structure occurred due to the recrystallization of amylopectin, whereas the VH-type structure occurred due to the crystallization of amylase [77]. The intensity of these peaks increased with the incorporation of CNFs, suggesting an overall increase in the crystallinity of the composites [30]. However, the peak position did not change or disappear. The results confirmed that the incorporation of CNFs did not change the crystalline structure of TPS. Therefore, the marked increase in peak height at 22° was attributed to CNFs in TPS. The elaborated TPS/CNF composites are not fully amorphous, according to the XRD study, and the crystallinity is caused by the retrogradation of TPS plasticized with glycerol [78].

Table 5
Thermal properties CNF reinforced TPS composites.

Samples	T_5 (°C)	T50 (°C)	Tmax (°C)	Residue at 500 °C
Neat starch	62.28	301.16	307.32	5.723
TPS/CNF 1	92.67	314.61	323.88	8.747
TPS/CNF 2	71.08	305.45	311.38	9.766
TPS/CNF 3	67.48	304.94	312.16	9.123
TPS/CNF 4	61.31	304.71	308.35	8.518

3.2.3. Thermal properties of TPS/CNF nanocomposite

The thermal stability of the developed polymer nanocomposite films could be studied using thermal degradation curves from thermogravimetric analysis (TGA). Besides, DSC studies were also performed. The TG, DTG, and DSC thermograms of TPS/CNF composites are shown in Fig. 5. The TG and DTG curves (Fig. 5A and B) of the nanocomposites showed three degradation steps, according to previous studies based on starch biocomposite films [71]. The first degradation between 100 and 200 °C is due to the evaporation of weakly bonded water molecules, followed by glycerol [79]. The second degradation at ~300 °C is due to the degradation of thermoplastic starch and CNFs [80]. At last, the third

Table 6
Tensile strength, elongation at break, and Young's modulus for neat starch and TPS/CNF composites.

Sample	Tensile strength (MPa)	Elongation at break (%)	Young's modulus (MPa)
Neat starch	1.77 ± 0.30	31.36 ± 4.12	15.82 ± 1.12
TPS/CNF 1	3.14 ± 0.62	38.82 ± 2.60	24.62 ± 1.18
TPS/CNF 2	3.63 ± 0.19	53.01 ± 5.12	24.70 ± 1.29
TPS/CNF 3	4.62 ± 0.42	29.82 ± 4.37	42.35 ± 1.45
TPS/CNF 4	3.98 ± 0.56	29.86 ± 4.72	50.45 ± 1.62

degradation at ~520 °C is due to the decomposition of lignin and carbonaceous residue [71].

Table 5 shows T_5, T_{50}, T_{max}, and the residue at 500 °C of the CNF reinforced TPS composites obtained from the TG and DTG thermograms. The addition of CNFs to the thermoplastic starch matrix showed an increase in T_5, T_{50}, T_{max}, and the residue at 500 °C due to the strong intermolecular hydrogen bonding between the CNFs and TPS [82]. Note that both CNFs and TPS are hydrophilic. This result confirms that the incorporation of CNFs enhanced the thermal stability of TPS. The immobilization of amylopectin chains by the CNFs is responsible for the increased onset degradation temperature of the developed composites. The accumulation of glycerol in the interfacial boundary of CNF/amylopectin favours the formation of crystallites of amylopectin around CNFs [83]. The formation of these crystallites also improves the thermal stability of the prepared composites. It is worth mentioning that 1 wt% CNF reinforced composites showed the highest thermal stability. On the other hand, at higher concentrations, the CNFs may tend to agglomerate due to the weak Van der Waals forces existing between them and, hence the compatibility of the filler with polymer matrix will be reduced and cause more defects, thus reducing the thermal stability of the composites.

Differential scanning calorimetric studies were also carried out to analyze TPS/CNF composites (Fig. 5C). Two endothermic peaks were observed in the DSC thermogram. The first endothermic peak at ~100 °C is due to the evaporation of water molecules present in the composite samples [81]. The second endothermic peak is due to the decomposition of the TPS and CNFs [71]. These results are according to TGA thermograms. Because of the low value of the heat capacity change, determining the glass transition temperatures (T_g) of the produced composites from DSC analysis is difficult [78].

3.2.4. Mechanical properties of TPS/CNF Nanocomposites

The representative tensile stress-strain curve of neat TPS and CNF reinforced TPS are shown in Fig. 5D. Besides, tensile strength, elongation at break and Young's modulus are shown in Table 6.

The stress-strain curve showed some changes in tensile strength, modulus, and elongation at the break of the TPS composites concerning the concentration of CNFs. The neat TPS films had poor tensile properties, limiting the commercial application of starch-based films [71]. According to Table 6, about 161% improvement in the tensile strength was observed when neat TPS was reinforced with 3 wt% CNFs. The increase in the tensile strength of the prepared composite films was possibly due to the reinforcement of the CNFs with the TPS matrix. The reinforcing effect of the CNFs with the TPS matrix is due to the intermolecular hydrogen bonding interaction between CNFs and TPS [84]. Thus, the interfacial adhesion between the CNFs and starch matrix is good and offered strong fiber reinforcement. In addition, the number of defects/porosities of the TPS matrix could be reduced with the incorporation of CNFs. CNFs may occupy the defect sites in the polymer matrix, resulting in a more compact structure for the composites. Besides, the nanosize and high surface area of CNFs cause effective surface bonding with the TPS matrix. The hydrogen-bonded network structure formed between CNFs and starch could improve the system's rigidity, which helps to transfer the stress effectively due to the superior tensile strength of TPS/CNF composites. The marginal decrease in the tensile strength at 4 wt% CNF loading may be due to the agglomeration and dispersion issue of CNFs.

As presented in Table 6, the elongation at break was minimum for TPS/CNF 3 composite due to the effective immobilization of starch polymer chains by CNFs. Hietala and co-workers observed a similar trend in elongation at break when potato starch is reinforced with wood flour derived CNFs [85]. Besides, according to Table 6, about 218% improvement in Young's modulus is observed when 4 wt% CNFs is incorporated into neat TPS. The high stiffness of CNFs and their good interaction with the TPS matrix account for the rise in Young's modulus in the prepared TPS/CNF composites. The high modulus of CNFs (140 GPa) in comparison to the TPS matrix (87 MPa) is also responsible for the increase in Young's modulus of the elaborated biocomposites [86]. The promising interaction between CNFs and TPS is depicted in Fig. 6.

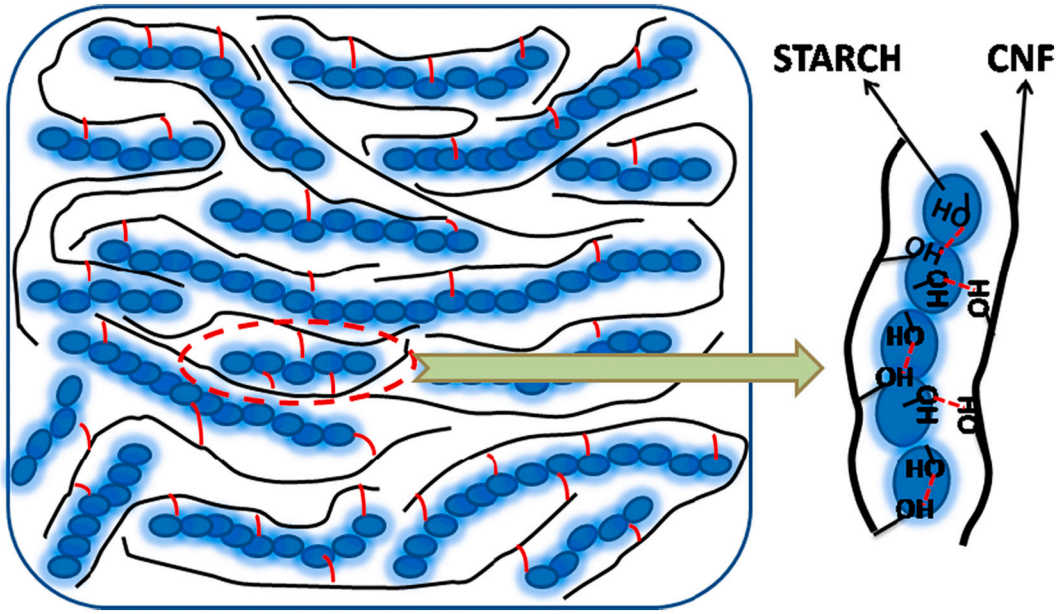

Fig. 6. Sketch of plausible hydrogen bonding interaction between CNFs and TPS matrix.

Fazeli and co-workers reported similar tensile strength and elastic modulus improvement when TPS is reinforced with CNFs [87].

4. Conclusion

The study reports the successful isolation of CNFs from the roots of *Chrysopogon zizanioides* for the first time using a chlorine-free extraction method. The successful removal of hemicellulose, lignin, pectin, and wax from the raw *Chrysopogon zizanioides* fibers was confirmed by FTIR and XRD analysis. The XRD pattern showed the formation of Type-I nanocellulose with a high crystallinity index of 65.08%. The diameter of CNFs was found to be in the range of 17–27 nm by TEM analysis, which was validated by DLS analysis. The T_{50} and T_{max} of CNFs increased by 9 °C and 7 °C respectively, when compared to raw fibers, owing to the produced CNFs' improved thermal stability. The solvent casting process was used to make the TPS/CNF bionanocomposite films. When compared to neat TPS, the tensile strength of a 3 wt% CNF reinforced composite was increased by 161%. The efficient immobilization of starch polymer chains by the CNFs was also demonstrated by the decrease in elongation at break and an increase in the elastic modulus of TPS/CNF composites at high fiber loading. The hydrogen bonding interaction between CNFs and starch was responsible for improving the tensile properties of TPS/CNF composite films, which the FTIR-ATR, XRD analysis further confirmed. The prepared TPS/CN composite films can be used for packaging applications based on the presented results. The swelling, barrier (oxygen and water vapor permeability), biodegradability, and antibacterial studies will be conducted shortly to utilize these green composite films in sustainable, intelligent packaging applications effectively.

CRediT authorship contribution statement

Midhun Dominic C.D.: Conceptualization, Methodology, Visualization, Writing- Original draft. **P.M. Sabura Begum**: Supervision. **Athira S. Kumar**: Investigation. **Neenu K.V.**: Investigation. **Divya Dinakaran**: Investigation. **Effina John**: Investigation. **Jaison M. Joy**.: Investigation. **Donna Baby**: Data curation. **Meenu Mariya Thomas**: Data curation. **Derval dos Santos Rosa**: Writing, Reviewing and Editing. **Jyotishkumar Parameswaranpillai**: Writing, Reviewing and Editing. **Mohammad Reza Saeb**: Methodology, Writing, Reviewing and Editing. **Paulo Henrique Camani**: Writing and Reviewing.

Declaration of competing interest

The authors declare no conflicts of interest.

Acknowledgment

The authors greatly acknowledge Sacred Heart College (Autonomous), Thevara, Kochi for the seed money grant No.C.11/RES/2016, No.D.20/RES/2017, and No.G.1/RES/2020. The authors would like to thank SAIF STIC, CUSAT for chemical analysis. In addition, the authors thank the São Paulo Research Foundation (FAPESP) (2019/16301-6 and 2018/11277-7).

References

[1] C. Ngaowthong, M. Borůvka, L. Běhálek, P. Lenfel, M. Švec, R. Dangtungee, S. Siengchin, S.M. Rangappa, J. Parameswaranpillai, Recycling of sisal fiber reinforced polypropylene and polylactic acid composites: thermo-mechanical properties, morphology, and water absorption behavior, Waste Manag. 97 (2019) 71–81, https://doi.org/10.1016/j.wasman.2019.07.038.

[2] S.A. Varghese, H. Pulikkalparambil, S.M. Rangappa, S. Siengchin, J. Parameswaranpillai, Novel biodegradable polymer films based on poly(3-hydroxybutyrate-co-3-hydroxyvalerate) and Ceiba pentandra natural fibers for packaging applications, Food Packag. Shelf Life 25 (2020), 100538, https://doi.org/10.1016/j.fpsl.2020.100538.

[3] E. Foschi, A. Bonoli, The commitment of packaging industry in the framework of the European strategy for plastics in a circular economy, Adm. Sci. 9 (2019) 18, https://doi.org/10.3390/admsci9010018.

[4] R. Shen, S. Xue, Y. Xu, Q. Liu, Z. Feng, H. Ren, H. Zhai, Research progress and development demand of nanocellulose reinforced polymer composites, Polymers 12 (2020) 1–19.

[5] M. Rajinipriya, M. Nagalakshmaiah, M. Robert, S. Elkoun, Homogenous and transparent nanocellulosic films from carrot, Ind. Crop. Prod. 118 (2018) 53–64, https://doi.org/10.1016/j.indcrop.2018.02.076.

[6] J. Huang, X. Ma, G. Yang, D. Alain, Introduction to nanocellulose, nanocellulose: from fundamentals to, Adv. Mater. (2019) 1–20, https://doi.org/10.1002/9783527807437.ch1.

[7] B. Thomas, M.C. Raj, B.K. Athira, H.M. Rubiyah, J. Joy, A. Moores, G.L. Drisko, C. Sanchez, Nanocellulose, a versatile green platform: from biosources to materials and their applications, Chem. Rev. 118 (2018) 11575–11625, https://doi.org/10.1021/acs.chemrev.7b00627.

[8] A. Kumar, Y. Singh Negi, V. Choudhary, N. Kant Bhardwaj, Characterization of cellulose nanocrystals produced by acid-hydrolysis from sugarcane bagasse as agro-waste, J. Mater. Phys. Chem. 2 (2020) 1–8, https://doi.org/10.12691/jmpc-2-1-1.

[9] M. Mahardika, H. Abral, A. Kasim, S. Arief, M. Asrofi, Production of nanocellulose from pineapple leaf fibers via high-shear homogenization and ultrasonication, Fibers 6 (2018) 1–12, https://doi.org/10.3390/fib6020028.

[10] A. de Campos, A.C. Correa, D. Cannella, E.de M. Teixeira, J.M. Marconcini, A. Dufresne, L.H.C. Mattoso, P. Cassland, A.R. Sanadi, Obtaining nanofibers from curauá and sugarcane bagasse fibers using enzymatic hydrolysis followed by sonication, Cellulose 20 (2013) 1491–1500, https://doi.org/10.1007/s10570-013-9909-3.

[11] J.B. Ali, A. Danladi, M.M. Bukhari, B.B. Nyakuma, P. Mamza, Z.B. Mohamad, A. B. Musa, I.M. Inuwa, Extraction and characterization of cellulose nanofibres and cellulose nanocrystals from Sammaz-14 maize cobs, J. Nat. Fibers 00 (2020) 1–16, https://doi.org/10.1080/15440478.2020.1856279.

[12] L. Ravindran, M.S. Sreekala, S. Thomas, Novel processing parameters for the extraction of cellulose nanofibres (CNF) from environmentally benign pineapple leaf fibres (PALF): structure-property relationships, Int. J. Biol. Macromol. 131 (2019) 858–870, https://doi.org/10.1016/j.ijbiomac.2019.03.134.

[13] A. Chakraborty, M. Sain, M. Kortschot, Cellulose microfibrils: a novel method of preparation using high shear refining and cryocrushing, Holzforschung 59 (2005) 102–107, https://doi.org/10.1515/HF.2005.016.

[14] S. Nie, C. Zhang, Q. Zhang, K. Zhang, Y. Zhang, P. Tao, S. Wang, Enzymatic and cold alkaline pretreatments of sugarcane bagasse pulp to produce cellulose nanofibrils using a mechanical method, Ind. Crop. Prod. 124 (2018) 435–441, https://doi.org/10.1016/j.indcrop.2018.08.033.

[15] C. Liu, B. Li, H. Du, D. Lv, Y. Zhang, G. Yu, X. Mu, H. Peng, Properties of nanocellulose isolated from corncob residue using sulfuric acid, formic acid, oxidative and mechanical methods, Carbohydr. Polym. 151 (2016) 716–724, https://doi.org/10.1016/j.carbpol.2016.06.025.

[16] R.J. Moon A. Martini J. Nairn J. Youngblood A. Martini J. Nairn Cellulose nanomaterials review: structure, properties and nanocomposites, Chem. Soc. Rev., 40(7), pp. 3941–3994. doi:10.1039/c0cs00108b.

[17] H. Xie, H. Du, X. Yang, C. Si, Recent strategies in preparation of cellulose nanocrystals and cellulose nanofibrils derived from raw cellulose materials, Int. J. Polym. Sci. 2018 (2018), 7923068, https://doi.org/10.1155/2018/7923068.

[18] Y.W. Chen, H.V. Lee, S.B. Abd Hamid, Preparation and characterization of cellulose crystallites via Fe(III)-, Co(II)- and Ni(II)-assisted dilute sulfuric acid catalyzed hydrolysis process, J.Nano Res. 41 (2016) 96–109, https://doi.org/10.4028/www.scientific.net/JNanoR.41.96.

[19] C.J. Chirayil, J. Joy, L. Mathew, M. Mozetic, J. Koetz, S. Thomas, Isolation and characterization of cellulose nanofibrils from Helicteres isora plant, Ind. Crop. Prod. 59 (2014) 27–34, https://doi.org/10.1016/j.indcrop.2014.04.020.

[20] B.M. Cherian, A.L. Leão, S.F. de Souza, S. Thomas, L.A. Pothan, M. Kottaisamy, Isolation of nanocellulose from pineapple leaf fibres by steam explosion, Carbohydr. Polym. 81 (2010) 720–725, https://doi.org/10.1016/j.carbpol.2010.03.046.

[21] P. Balakrishnan, M.S. Sreekala, M. Kunaver, M. Huskić, S. Thomas, Morphology, transport characteristics and viscoelastic polymer chain confinement in nanocomposites based on thermoplastic potato starch and cellulose nanofibers from pineapple leaf, Carbohydr. Polym. 169 (2017) 176–188, https://doi.org/10.1016/j.carbpol.2017.04.017.

[22] E. Tavassoli-Kafrani, M.V. Gamage, L.F. Dumée, L. Kong, S. Zhao, Edible films and coatings for shelf life extension of mango: a review, Crit. Rev. Food Sci. Nutr. (2020) 1–29, https://doi.org/10.1080/10408398.2020.1853038.

[23] A. Edhirej, S.M. Sapuan, M. Jawaid, N.I. Zahari, Effect of various plasticizers and concentration on the physical, thermal, mechanical, and structural properties of cassava-starch-based films, Starch-Stärke 69 (2016) 1500366, https://doi.org/10.1002/star.201500366.

[24] J.C. Canto, V.M. Moo-huchin, Thermoplastic starch (TPS)-cellulosic fibers composites: mechanical properties and water vapor barrier: a review, in: Composites From Renewable and Sustainable Materials 85, 2016, https://doi.org/10.5772/65397.

[25] A. Dufresne, D. Danièle, R. V. Michel, Cellulose microfibrils from potato tuber cells: processing and characterization of starch – cellulose microfibril composites, J. Appl. Polym. Sci. 76 (1999) 2080–2092.

[26] E.de M. Teixeira, D. Pasquini, A.A.S. Curvelo, E. Corradini, M.N. Belgacem, A. Dufresne, Cassava bagasse cellulose nanofibrils reinforced thermoplastic cassava

starch, Carbohydr. Polym. 78 (2009) 422–431, https://doi.org/10.1016/j.carbpol.2009.04.034.
[27] N.R. Savadekar, S.T. Mhaske, Synthesis of nano cellulose fibers and effect on thermoplastics starch based films, Carbohydr. Polym. 89 (2012) 146–151, https://doi.org/10.1016/j.carbpol.2012.02.063.
[28] P. Balakrishnan, S. Gopi, M.S. Sreekala, S. Thomas, UV resistant transparent bionanocomposite films based on potato starch/cellulose for sustainable packaging, Starch/Staerke 70 (2018) 1–34, https://doi.org/10.1002/star.201700139.
[29] J.C. Cerqueira, J. Da Silva Penha, R.S. Oliveira, L.L. Nani Guarieiro, P. Da Silva Melo, J.D. Viana, B.A. Souza Machado, Production of biodegradable starch nanocomposites using cellulose nanocrystals extracted from coconut fibers, Polimeros 27 (2017) 320–329, https://doi.org/10.1590/0104-1428.05316.
[30] C.C.de S. Coelho, R.B.S. Silva, C.W.P. Carvalho, A.L. Rossi, J.A. Teixeira, O. Freitas-Silva, L.M.C. Cabral, Cellulose nanocrystals from grape pomace and their use for the development of starch-based nanocomposite films, Int. J. Biol. Macromol. 159 (2020) 1048–1061, https://doi.org/10.1016/j.ijbiomac.2020.05.046.
[31] N. Nordin, S.H. Othman, R. Kadir Basha, S. Abdul Rashid, Mechanical and thermal properties of starch films reinforced with microcellulose fibres, Food Res. 2 (2018) 555–563, https://doi.org/10.26656/fr.2017.2(6).110.
[32] J.S. Santana, J.M. do Rosário, C.C. Pola, C.G. Otoni, N. de Fátima FerreiraSoares, G. P. Camilloto, R.S. Cruz, Cassava starch-based nanocomposites reinforced with cellulose nanofibers extracted from sisal, J. Appl. Polym. Sci. 134 (2017) 1–9, https://doi.org/10.1002/app.44637.
[33] A.V. Kiruthika, A review on physico-mechanical properties of bast fibre reinforced polymer composites, J. Build. Eng. 9 (2017) 91–99, https://doi.org/10.1016/j.jobe.2016.12.003.
[34] S. Donjadee, T. Tingsanchali, Soil and water conservation on steep slopes by mulching using rice straw and vetiver grass clippings, Agric. Nat. Resour. 50 (2016) 75–79, https://doi.org/10.1016/j.anres.2015.03.001.
[35] N. Roongtanakiat, S. Tangruangkiat, R. Meesat, Utilization of vetiver grass (Vetiveria zizanioides) for removal of heavy metals from industrial wastewaters, ScienceAsia 33 (2007) 397–403, https://doi.org/10.2306/scienceasia1513-1874.2007.33.397.
[36] K.A. Santos, E.J. Klein, C. da Silva, E.A. da Silva, L. Cardozo-Filho, Extraction of vetiver (Chrysopogon zizanioides) root oil by supercritical CO2, pressurized-liquid, and ultrasound-assisted methods and modeling of supercritical extraction kinetics, J. Supercrit. Fluids 150 (2019) 30–39, https://doi.org/10.1016/j.supflu.2019.04.005.
[37] N. Singh, V.R. Singh, R.K. Lal, R.S. Verma, A. Mishra, R. Yadav, Quantification of genotypic and chemotypic diversity for elite clone selection with high-quality essential oil traits in vetiver [Chrysopogon zizanioides (L.) Roberty], J. Essent. Oil-Bearing Plants 22 (2019) 1150–1162, https://doi.org/10.1080/0972060X.2019.1661795.
[38] A.L.M.P. Leite, C.D. Zanon, F.C. Menegalli, Isolation and characterization of cellulose nanofibers from cassava root bagasse and peelings, Carbohydr. Polym. 157 (2017) 962–970, https://doi.org/10.1016/j.carbpol.2016.10.048.
[39] M. Szymanska-Chargot, M. Chylinska, K. Gdula, A. Koziol, A. Zdunek, Isolation and characterization of cellulose from different fruit and vegetable pomaces, Polymers 9 (2017) 495, https://doi.org/10.3390/polym9100495.
[40] H. Chen, W. Zhang, X. Wang, H. Wang, Y. Wu, T. Zhong, B. Fei, Effect of alkali treatment on wettability and thermal stability of individual bamboo fibers, J. Wood Sci. 64 (2018) 398–405, https://doi.org/10.1007/s10086-018-1713-0.
[41] A. De Souza, S. Panthapulakkal, S. Kumar, M. Sain, L. Bufalinof, J. Raabe, I. Paula, D.A. Miranda, M. Alice, Improving cellulose nanofibrillation of non-wood fiber using alkaline and bleaching pre-treatments, Ind. Crops Prod. 131 (2019) 203–212, https://doi.org/10.1016/j.indcrop.2019.01.046.
[42] I.M. Fareez, N.A. Ibrahim, W.M.H. Wan Yaacob, N.A. Mamat Razali, A.H. Jasni, F. Abdul Aziz, Characteristics of cellulose extracted from josapine pineapple leaf fibre after alkali treatment followed by extensive bleaching, Cellulose 25 (2018) 4407–4421, https://doi.org/10.1007/s10570-018-1878-0.
[43] S.K. Thomas, P.M.S. Begum, C.D.Midhun Dominic, N.V. Salim, N. Hameed, S. M. Rangappa, S. Siengchin, J. Parameswaranpillai, Isolation and characterization of cellulose nanowhiskers from Acacia caesia plant, J. Appl. Polym. Sci. 138 (2021), https://doi.org/10.1002/app.50213.
[44] Y.W. Chen, H.V. Lee, S.B.A. Hamid, Preparation of nanostructured cellulose via Cr (III)- and Mn(II)-transition metal salt catalyzed acid hydrolysis approach, Bioresources 11 (2016) 7224–7241, https://doi.org/10.15376/biores.11.3.7224-7241.
[45] P.H.F. Pereira, H.L. Ornaghi Júnior, L.V. Coutinho, B. Duchemin, M.O.H. Cioffi, Obtaining cellulose nanocrystals from pineapple crown fibers by free-chlorite hydrolysis with sulfuric acid: physical, chemical and structural characterization, Cellulose 27 (2020) 5745–5756, https://doi.org/10.1007/s10570-020-03179-6.
[46] H. Dai, S. Ou, Y. Huang, H. Huang, Utilization of pineapple peel for production of nanocellulose and film application, Cellulose 25 (2018) 1743–1756, https://doi.org/10.1007/s10570-018-1671-0.
[47] R.C.N.R. Corrales, F.M.T. Mendes, C.C. Perrone, C. Santanna, W. De Souza, Y. Abud, E.P.D.S. Bon, V. Ferreira-Leitão, Structural evaluation of sugar cane bagasse steam pretreated in the presence of CO2 and SO2, Biotechnol. Biofuels 5 (2012) 1–8, https://doi.org/10.1186/1754-6834-5-36.
[48] M.K.M. Haafiz, A. Hassan, H.P.S. Abdul Khalil, A.F. Owolabi, M.M. Marliana, R. Arjmandi, I.M. Inuwa, M.R. Nurul Fazita, M.H. Hussin, Cellulose nanowhiskers from oil palm empty fruit bunch biomass as green fillers, in: Cellulose-reinforced Nanofibre Composites: Production, Properties and Applications, 2017, pp. 241–259, https://doi.org/10.1016/B978-0-08-100957-4.00010-3.
[49] A. Bahloul, Z. Kassab, M. El Bouchti, H. Hannache, A. El, K. Qaiss, M. Oumam, M. El Achaby, Micro- and nano-structures of cellulose from eggplant plant (Solanum melongena L) agricultural residue, Carbohydr. Polym. 253 (2021), 117311, https://doi.org/10.1016/j.carbpol.2020.117311.
[50] C. Trilokesh, P. Bavadharani, M. Mahapriyadarshini, R. Janani, K.B. Uppuluri, Recycling baby diaper waste into cellulose and nanocellulose, Waste Biomass Valorization (2020), https://doi.org/10.1007/s12649-020-01312-x.
[51] H.A. Foner, N. Adan, The characterization of papers by X-ray diffraction (XRD): measurement of cellulose crystallinity and determination of mineral composition, J. Forensic Sci. Soc. 23 (1983) 313–321, https://doi.org/10.1016/S0015-7368(83)72269-3.
[52] E. Abraham, B. Deepa, L.A. Pothan, M. Jacob, S. Thomas, U. Cvelbar, R. Anandjiwala, Extraction of nanocellulose fibrils from lignocellulosic fibres: a novel approach, Carbohydr. Polym. 86 (2011) 1468–1475, https://doi.org/10.1016/j.carbpol.2011.06.034.
[53] L.M. Moreno, S. Gorinstein, O.J. Medina, J. Palacios, E.J. Muñoz, Valorization of garlic crops residues as precursors of cellulosic materials, Waste Biomass Valorization 11 (2020) 4767–4779, https://doi.org/10.1007/s12649-019-00799-3.
[54] M. Dominic, R. Joseph, P.M. Sabura Begum, B.P. Kanoth, J. Chandra, S. Thomas, Green tire technology: effect of rice husk derived nanocellulose (RHNC) in replacing carbon black (CB) in natural rubber (NR) compounding, Carbohydr. Polym. 230 (2020) 115–620, https://doi.org/10.1016/j.carbpol.2019.115620.
[55] M. Dominic C.D., R. Joseph, P.M.S. Begum, M. Joseph, D. Padmanabhan, L. A. Morris, A.S. Kumar, K. Formela, Cellulose nanofibers isolated from the Cuscuta reflexa plant as a green reinforcement of natural rubber, Polymers 12 (2020) 814, https://doi.org/10.3390/polym12040814.
[56] A.F.Ireana Yusra, H. Juahir, N.W.N.A. Firdaus, A.H. Bhat, A. Endut, A. Khalil, G. Adiana, U. Sultan, Z. Abidin, U.T. Petronas, S. Iskandar, U. Sultan, Z. Abidin, B. Campus, U. Sains, Controlling of green nanocellulose fiber properties produced by chemo-mechanical treatment process via SEM, TEM, AFM and image analyzer characterization, J. Fundam. Appl. Sci. 10 (2018) 1–17.
[57] P. Panyasiri, N. Yingkamhaeng, N.T. Lam, P. Sukyai, Extraction of cellulose nanofibrils from amylase-treated cassava bagasse using high-pressure homogenization, Cellulose 25 (2018) 1757–1768, https://doi.org/10.1007/s10570-018-1686-6.
[58] K.O. Reddy, C. Uma Maheswari, E. Muzenda, M. Shukla, A.V. Rajulu, Extraction and characterization of cellulose from pretreated ficus (peepal tree) leaf fibers, J. Nat. Fibers 13 (2016) 54–64, https://doi.org/10.1080/15440478.2014.984055.
[59] A. Kumagai, N. Tajima, S. Iwamoto, T. Morimoto, A. Nagatani, T. Okazaki, T. Endo, Properties of natural rubber reinforced with cellulose nanofibers based on fiber diameter distribution as estimated by differential centrifugal sedimentation, Int. J. Biol. Macromol. 121 (2019) 989–995, https://doi.org/10.1016/j.ijbiomac.2018.10.090.
[60] F. Hu, J. Zeng, Z. Cheng, X. Wang, B. Wang, Z. Zeng, K. Chen, Cellulose nanofibrils (CNFs) produced by different mechanical methods to improve mechanical properties of recycled paper, Carbohydr. Polym. 254 (2021), 117474, https://doi.org/10.1016/j.carbpol.2020.117474.
[61] S. Chenampulli, G. Unnikrishnan, A. Sujith, S. Thomas, T. Francis, Cellulose nanoparticles from pandanus: viscometric and crystallographic studies, Cellulose 20 (2013) 429–438, https://doi.org/10.1007/s10570-012-9831-0.
[62] S. Ventura-cruz, A. Tecante, Extraction and characterization of cellulose nanofibers from rose stems (Rosa spp.), Carbohydr. Polym. 220 (2019) 53–59, https://doi.org/10.1016/j.carbpol.2019.05.053.
[63] P.P. Hanthong, M.A. Yufei, G.G. Uan, A.A. Budula, Extraction of nanocellulose from raw apple stem, J. Japan Inst. Energy (2015) 787–793.
[64] M. Yadav, R.S. Rengasamy, D. Gupta, Characterization of pearl millet (Pennisetum glaucum) waste, Carbohydr. Polym. 212 (2019) 160–168, https://doi.org/10.1016/j.carbpol.2019.02.034.
[65] F.M. Pelissari, P.J.D.A. Sobral, F.C. Menegalli, Isolation and characterization of cellulose nanofibers from banana peels, Cellulose 21 (2014) 417–432, https://doi.org/10.1007/s10570-013-0138-6.
[66] K.J. Nagarajan, A.N. Balaji, N.R. Ramanujam, SC, Carbohydr. Polym. (2019), https://doi.org/10.1016/j.carbpol.2019.02.063.
[67] E. Syafri, A. Kasim, H. Abral, A. Asben, Cellulose nanofibers isolation and characterization from ramie using a chemical-ultrasonic treatment, J. Nat. Fibers 16 (2019) 1145–1155, https://doi.org/10.1080/15440478.2018.1455073.
[68] Z. Hu, R. Zhai, J. Li, Y. Zhang, J. Lin, Preparation and characterization of nanofibrillated cellulose from bamboo fiber via ultrasonication assisted by repulsive effect, Int. J. Polym. Sci. 2017 (2017), https://doi.org/10.1155/2017/9850814.
[69] R. Sánchez, E. Espinosa, J. Domínguez-Robles, J.M. Loaiza, A. Rodríguez, Isolation and characterization of lignocellulose nanofibers from different wheat straw pulps, Int. J. Biol. Macromol. 92 (2016) 1025–1033, https://doi.org/10.1016/j.ijbiomac.2016.08.019.
[70] W. Chen, H. Yu, Y. Liu, Y. Hai, M. Zhang, P. Chen, Isolation and characterization of cellulose nanofibers from four plant cellulose fibers using a chemical-ultrasonic process, Cellulose 18 (2011) 433–442, https://doi.org/10.1007/s10570-011-9497-z.
[71] R. Bodirlau, C.A. Teaca, I. Spiridon, Influence of natural fillers on the properties of starch-based biocomposite films, Compos. Part B 44 (2013) 575–583, https://doi.org/10.1016/j.compositesb.2012.02.039.
[72] C.wei Zhang, S.S. Nair, H. Chen, N. Yan, R. Farnood, F.yi Li, Thermally stable, enhanced water barrier, high strength starch bio-composite reinforced with lignin containing cellulose nanofibrils, Carbohydr. Polym. 230 (2020), 115626, https://doi.org/10.1016/j.carbpol.2019.115626.

[73] M. Asrofi, H. Abral, A. Kasim, A. Pratoto, M. Mahardika, F. Hafizulhaq, Characterization of the sonicated yam bean starch bionanocomposites reinforced by nanocellulose water hyacinth fiber (WHF): the effect of various fiber loading, J. Eng. Sci. Technol. 13 (2018) 2700–2715.
[74] W.T. Owi, H.L. Ong, S.T. Sam, A.R. Villagracia, C.kuo Tsai, H.M. Akil, Unveiling the physicochemical properties of natural Citrus aurantifolia crosslinked tapioca starch/nanocellulose bionanocomposites, Ind. Crops Prod. 139 (2019), 111548, https://doi.org/10.1016/j.indcrop.2019.111548.
[75] J.I. Morán, A. Vázquez, V.P. Cyras, Bio-nanocomposites based on derivatized potato starch and cellulose, preparation and characterization, J. Mater. Sci. 48 (2013) 7196–7203, https://doi.org/10.1007/s10853-013-7536-x.
[76] S. Karimi, A. Dufresne, P.Md. Tahir, A. Karimi, A. Abdulkhani, Biodegradable starch-based composites: effect of micro and nanoreinforcements on composite properties, J. Mater. Sci. 49 (2014) 4513–4521, https://doi.org/10.1007/s10853-014-8151-1.
[77] J. Ren, K.M. Dang, E. Pollet, L. Avérous, Preparation and characterization of thermoplastic potato starch/halloysite nano-biocomposites: effect of plasticizer nature and nanoclay content, Polymers 10 (2018) 808, https://doi.org/10.3390/polym10080808.
[78] A. Orue, M.A. Corcuera, C. Peña, A. Eceiza, A. Arbelaiz, Bionanocomposites based on thermoplastic starch and cellulose nanofibers, J. Thermoplast. Compos. Mater. 29 (2016) 817–832, https://doi.org/10.1177/0892705714536424.
[79] A. Podshivalov, M. Zakharova, E. Glazacheva, M. Uspenskaya, Gelatin/potato starch edible biocomposite films: correlation between morphology and physical properties, Carbohydr. Polym. 157 (2017) 1162–1172, https://doi.org/10.1016/j.carbpol.2016.10.079.
[80] L. Averous, N. Boquillon, Biocomposites based on plasticized starch: thermal and mechanical behaviours, Carbohydr. Polym. 56 (2004) 111–122, https://doi.org/10.1016/j.carbpol.2003.11.015.
[81] G. Ayala, A. Agudelo, R. Vargas, Effect of glycerol on the electrical properties and phase behavior of cassava starch biopolymers, Dyna 79 (2012) 138–147.
[82] R.A. Ilyas, S.M. Sapuan, R. Ibrahim, H. Abral, M.R. Ishak, E.S. Zainudin, A. Atiqah, M.S.N. Atikah, E. Syafri, M. Asrofi, R. Jumaidin, Thermal biodegradability and water barrier properties of bio-nanocomposites based on plasticised sugar palm starch and nanofibrillated celluloses from sugar palm fibres, J. Biobased Mater. Bioenergy 14 (2019) 234–248, https://doi.org/10.1166/jbmb.2020.1951.
[83] A. Ghanbari, T. Tabarsa, A. Ashori, A. Shakeri, M. Mashkour, Preparation and characterization of thermoplastic starch and cellulose nanofibers as green nanocomposites: extrusion processing, Int. J. Biol. Macromol. 112 (2018) 442–447, https://doi.org/10.1016/j.ijbiomac.2018.02.007.
[84] H. Abral, A.S. Anugrah, F. Hafizulhaq, D. Handayani, E. Sugiarti, A.N. Muslimin, Effect of nanofibers fraction on properties of the starch based biocomposite prepared in various ultrasonic powers, Int. J. Biol. Macromol. 116 (2018) 1214–1221, https://doi.org/10.1016/j.ijbiomac.2018.05.067.
[85] M. Hietala, A.P. Mathew, K. Oksman, Bionanocomposites of thermoplastic starch and cellulose nanofibers manufactured using twin-screw extrusion, Eur. Polym. J. 49 (2013) 950–956, https://doi.org/10.1016/j.eurpolymj.2012.10.016.
[86] M. Alidadi-shamsabadi, T. Behzad, R. Bagheri, B. Nari-nasrabadi, Preparation and characterization of low-density polyethylene/thermoplastic starch composites reinforced by cellulose nanofibers, Polym. Compos. 36 (2014) 2309–2316, https://doi.org/10.1002/pc.
[87] M. Fazeli, M. Keley, E. Biazar, Preparation and characterization of starch-based composite films reinforced by cellulose nanofibers, Int. J. Biol. Macromol. 116 (2018) 272–280, https://doi.org/10.1016/j.ijbiomac.2018.04.186.